SOLID MATTER

E.A. ELISEEV

Institute for Problems of Materials Science, Nat. Acad. of Sci. of Ukraine
(3, Krzhizhanovs'kyi Str., Kyiv 03142, Ukraine; e-mail: eugene.a.eliseev@gmail.com)

INFLUENCE OF ELECTROCAPILLARITY ON THE WATER MENISCUS SHAPE IN THE ATOMIC FORCE MICROSCOPY

In the framework of the analytical theory of electrocapillarity phenomena that arise in atomic force microscopy (AFM) experiments, the formation of a water meniscus under the AFM probe has been considered, and its dependence on the applied voltage has been analyzed. The non-uniformity of the electric field produced by the AFM probe, the influences of gravitation forces on the meniscus height, and the dependence of the surface energy of a meniscus on its shape are taken into account self-consistently. The influence of a strong non-uniform electric field of the probe on the emergence conditions, size, and shape of the water meniscus is analyzed for the first time. The Euler–Lagrange partial differential equation and the corresponding boundary conditions making allowance for the non-uniform electric field of an AFM probe, the gravitation force, the meniscus surface tension, and the environmental humidity and describing the thermodynamics of the water meniscus formation in a self-consistent way are derived. The obtained numerical results are in agreement with known experimental data.

K e y w o r d s: electrocapillarity, atomic force microscopy, water meniscus, Euler–Lagrange equation.

1. Introduction

Scanning probe atomic force microscopy (AFM) [1] is a unique, very powerful, and, at the same time, widely applied method of researches dealing with the surface morphology of various materials, as well as relevant electric, magnetic, and mechanical forces [1]. Various modifications of this method make it possible to investigate the properties of the near-surface layer in an arbitrary medium (not only in a solid) ranging from organic polymers, biological RNA and DNA specimens, liquid crystals, ferromagnets, and ferroelectrics to metals, graphene, and diamond. In the modern AFM, the surface morphology and the forces are studied with the nano-, subnano-, and even atomic resolution. This is a considerable advantage in comparison with ordinary optical microscopy, the resolution of which is determined by half an optical wavelength (about 250–400 nm). The resolution of the AFM operating in the topographical mode is determined by the curvature radius of the probe tip (about 5–25 nm for modern probes). Force and current measurements are characterized by a considerably better resolution owing to the dielectric enhancement effect for electric fields, because, while estimating the resolution, the probe curvature radius is multiplied by the dielectric permittivity of the medium around the probe ($\varepsilon \lesssim 10$) and divided by the effective dielectric permittivity of the specimen, which can largely exceed unity [2].

The atomic force microscope was invented by Calvin Quate and Christoph Gerber in 1986, almost immediately after the invention of the scan-

---

[1] Below, the abbreviation AFM is used for both the atomic force microscopy and the atomic force microscope, depending on the context.

ning tunnel microscope by Gerd Binnig and Heinrich Rohrer in 1982. This device is intended for studying the atomic structure of the surface. It consists of a probe and a mirror, the both being mounted on a cantilever, a light source (laser), a quadrant photodetector, and an electronic amplifier. A light beam produced by the laser falls on the mirror and is reflected to the photodetector. The latter, using the amplification system, transforms the probe vibrations into electric current oscillations (see Fig. 1).

Both the quantitative and qualitative interpretations of experimental results obtained with the use of AFM methods (in particular, the force structure and the screening of electric fields), as well as their resolution, substantially depend on the probe environment. A possibility or a requirement to carry out AFM experiments in the vacuum or a nonpolar medium (of the inert-gas type) is not always available, because the corresponding preparation procedure is expensive, long-term, and often inexpedient; especially in the case where the surface has to be studied under "environmental conditions". The overwhelming majority of AFM experiments are performed in the air environment with a humidity from 30 to 90%. It was found experimentally and shown theoretically that, if the air humidity exceeds 40%, superthin layers of water are condensed on hydrophilic surfaces, which are typical of the overwhelming majority of metals, semiconductors, ferroelectrics, and ferromagnets. In the damp air, a water meniscus several hundreds of nanometers and even several micrometers in height can easily be formed between the hydrophilic surfaces of the metal probe and the specimen owing to the capillary effects [3]. If an electric voltage is applied to the probe, water starts to be pulled into the region of the non-uniform electric field created by the probe (Fig. 2). It is natural that the conditions of meniscus formation, as well as the meniscus parameters, depend on the voltage applied to the probe.

The literature analysis [4, 5] revealed that the self-consistent theory of electrocapillarity phenomena in the AFM, although being challenging, had been developed insufficiently. As a rule, the authors consider either the cases where no electric voltage is applied to the probe and the meniscus is essentially spherical [4] or the case of a flat capacitor with a uniform electric field [5]. Some authors, instead of finding the real shape and parameters of the meniscus, assume it to be cylindrical [6]. Moreover, in those works, no
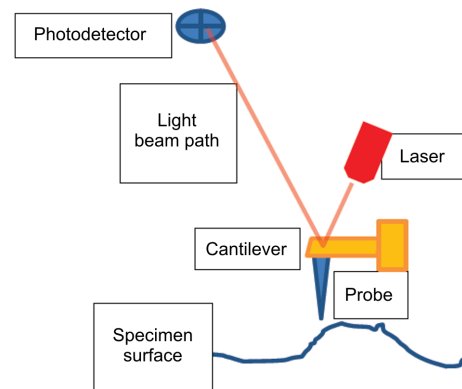

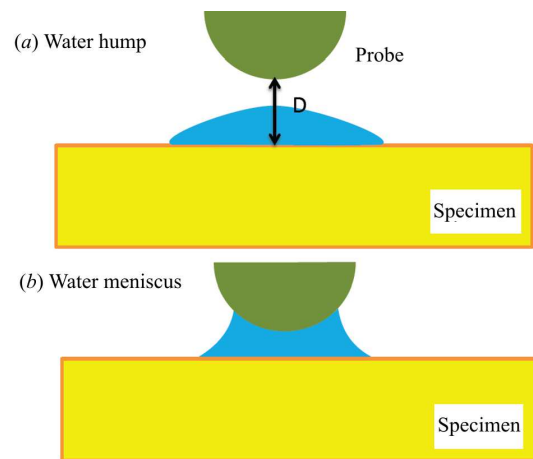**Fig. 1.** Schematic diagram of the scanning atomic force microscope (AFM)

Fig. 2. Water hump "pulled in" by the probe electric field *a*. Gravitation counteracts this process and "spread" the meniscus along the hydrophilic surface of the specimen. Water meniscus formed under the probe, when the latter approaches the surface or when the electric voltage applied to the probe increases *b*

gravitation force was taken into account, which can considerably affect the dimensions of the meniscus when it achieves micron heights.

The facts presented above served an impetus for this work. Here, a self-consistent analytical theory of the electrocapillarity phenomenon in the AFM experiment, namely, the formation of a water meniscus under the AFM probe tip, is developed, and the influence of the electric voltage applied to the probe is analyzed. The work is aimed at making allowance for the electrocapillarity phenomena in the non-uniform electric field of AFM probe, the influence of the grav-
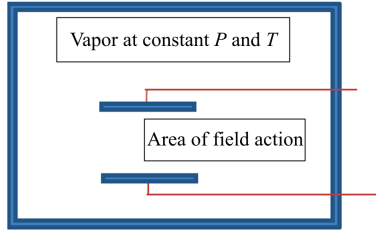
Fig. 3. Water vapor condensation in the electric field

itation force on the water meniscus height, and the dependence of the surface energy of the meniscus on its real shape, which must be determined self-consistently. This formulation of the problem, which takes into account the most important experimental factors, is relevant for both basic researches and applications, because, in most cases, even for microscopes with protective caps, the environmental humidity turns out sufficiently high for water to condense in the nanometer-sized gap between the probe and the studied surface.

2. Capillary Forces and Kelvin Equation

Plenty of substances are transformed from the vapor state into the liquid one in small cracks and pores. This phenomenon is called the capillary condensation. It originates forn the pressure difference under the curved surface and above it, which equals [7–9]

$$\Delta P = \gamma \left(\frac{1}{R_1} + \frac{1}{R_2} \right), \tag{1}$$

where γ is the surface tension coefficient, and R_1 and R_2 are the principal radii of curvature of the surface. This equality often referred to as the Young–Laplace formula [9]. Analyzing the problem from the thermodynamic viewpoint, one can understand that the pressure difference brings about a variation in the free energy of the system. Provided that the temperature T and the molar volume V_μ are constant, this variation can be written as follows:

$$\Delta G_{\mu p} = V_\mu \delta P = V_\mu \gamma \left(\frac{1}{R_1} + \frac{1}{R_2} \right). \tag{2}$$

Using the equation of state for the ideal gas, $PV_\mu = RT$, where R is the universal gas constant, we obtain that $dG_{\mu p} = RT \frac{dP}{P}$. Integrating this expression, we have $G_{\mu p} = G_0 + RT \ln \left(\frac{P}{P_0} \right)$. Then, from Eq. (2),

taking into account that $G_{\mu p} - G_0 = \Delta G_{\mu p}$, we obtain the Kelvin equation [10]

$$RT \ln \left(\frac{P}{P_0} \right) = \gamma V_\mu \left(\frac{1}{R_1} + \frac{1}{R_2} \right), \tag{3}$$

where P_0 is the normal pressure above a flat surface of vapor, and P the pressure outside the liquid surface. From this equation, if T and $\frac{P}{P_0}$ are known, one can find the so-called Kelvin radius r_K[10]:

$$r_K^{-1} = \gamma \left(\frac{1}{R_1} + \frac{1}{R_2} \right) = \frac{RT}{\gamma V_\mu} \ln \left(\frac{P}{P_0} \right). \tag{4}$$

The Kelvin equation was applied in work [4] to determine the shape of a meniscus formed under the AFM probe.

3. Kelvin Equation Making Allowance for the Electrocapillarity Effect

The Kelvin equation, in which the electrocapillarity effect in a uniform electric field was taken into account, but the contribution made by the potential energy of the gravitation force was neglected, was derived in work [5]. The density of the electrostatic energy (the energy per unit volume) looks like

$$u = \frac{\varepsilon \varepsilon_0}{2} E^2, \tag{5}$$

where $\varepsilon_0 = 8.85 \times 10^{-12}$ F/m is the electric constant (the vacuum permittivity), ε the relative dielectric permittivity of the medium, and E the electric field strength.

Let us consider a condenser system that is in contact with vapor at the pressure P. The pressure of saturated vapor in the absence of electric field equals P_0. At first, let $P < P_0$, i.e. the vapor is not condensed. Now, let an electric field be applied in a certain volume of vapor (Fig. 3). The condensation must evidently begin in this volume, because excess (5) of the electric energy (the principle of conservatism of the system) has to be compensated by reducing the number of free molecules.

The Gibbs thermodynamic potential δG_μ changes when the substance is "pulled" into the region of a strong electric field (condensation in the field). The corresponding variation per mole can be written as follows:

$$\Delta G_{\mu E} = -\frac{(\varepsilon - 1)\varepsilon_0}{2} E^2 V_\mu. \tag{6}$$

If the system is in the equilibrium state, the Gibbs energy for liquid equals the Gibbs energy for vapor. In the case of vapor, this energy depends on the pressure, and the balance equation in the absence of an electric field looks like [5]

$$G_\mu = G_0 + RT \ln P_{E0}, \qquad (7)$$

where the term G_0 does not depend on the pressure. In the region of electric field action, Eq. (7) reads [5]

$$G_{mE} = G_{m_0} + RT \ln P_{E0}. \qquad (8)$$

At equilibrium, the variation of the Gibbs energy for vapor is equal to that for liquid; i.e. $G_{\mu E} - G_0 = \Delta G_{\mu E}$ and

$$\ln \left(\frac{P_{E0}}{P_0} \right) = -\frac{V_\mu (\varepsilon - 1)\varepsilon_0 E^2}{2RT}. \qquad (9)$$

Since $\varepsilon > 1$ for any liquid, the right-hand side of Eq. (9) is always negative, and the pressure of saturated vapor diminishes in the electric field.

Expression (9) is valid only for plane liquid surfaces. To take the effect of surface bending into account, we should add the term $\gamma V_\mu C$ to its right-hand side. Here, C is the surface bending described by two principal radii of curvature, R_1 and R_2: $C = 1/R_1 + 1/R_2$. The bending of a concave surface is considered to be positive, and that of a convex surface to be negative. The surface bending results in the pressure change [5],

$$\ln \left(\frac{P_{E0}}{P_0} \right) = -\frac{V_\mu}{RT} \left[\frac{(\varepsilon - 1)\varepsilon_0 E^2}{2} - \gamma \left(\frac{1}{R_1} + \frac{1}{R_2} \right) \right]. \qquad (10)$$

Equation (10) is the modified Kelvin equation, in which the influence of a uniform electric field on the shape of a spherical meniscus is taken into account. However, it does not make allowance for a local variation of the meniscus shape and the gravitation force.

4. Non-Uniformity of Electric Field Created by the AFM Probe. Model of Effective Point Charge

Let us modify the approach applied in Section 3 and take into consideration that the electric field of the
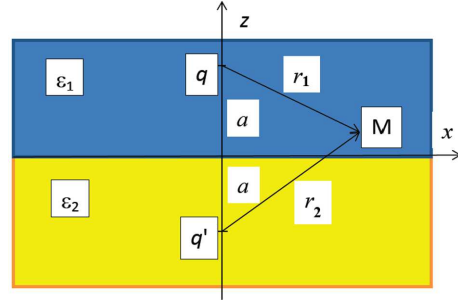
Fig. 4. Point charge q near the interface between two insulators and its image q'

AFM probe is strongly non-uniform. In the framework of the effective point charge model, when the electric field of the probe is approximated by the field of an effective point charge with an accuracy sufficient for the semiquantitative analysis [11], the problem is reduced to the known problem dealing with the field of an electric point charge near the interface between two dielectric media. In this case, the tensor of the specimen dielectric permittivity can be anisotropic, and this variant was analyzed in work [12]. For the sake of simplicity and to make the result more illustrative, the specimen in the presented work was considered in the isotropic-insulator approximation.

The magnitude q of the effective charge, the field of which approximates the field of the probe, is proportional to the electric voltage U applied to the probe. The corresponding coefficient of proportionality (the mutual capacitance) depends on the spatial region, in which the probe field is intended to be the best approximated.

The solutions of the problem concerning the electric potential of a point charge q near the interface of two insulators look like [13]

$$\varphi_1(z > 0) = \frac{q}{4\pi\varepsilon_0\varepsilon_1 r_1} + \frac{\varepsilon_1 - \varepsilon_2}{\varepsilon_1 + \varepsilon_2} \frac{q}{4\pi\varepsilon_0\varepsilon_1 r_2}, \qquad (11a)$$

$$\varphi_2(z < 0) = \frac{2}{(\varepsilon_1 + \varepsilon_2)} \frac{q}{4\pi\varepsilon_0 r_1}. \qquad (11b)$$

The dielectric permittivity of the medium equals ε_1 at $z > 0$ and ε_2 at $z < 0$. The choice of vectors $\mathbf{r}_1 = (x, y, z+a)$ and $\mathbf{r}_{21} = (x, y, z-a)$ is shown in Fig. 4.

The electric field $\mathbf{E} = -\nabla\varphi_1$ for the potential distribution (11a) is non-uniform. In particular,

$$E_x = -\frac{\partial}{\partial x}\varphi_1 = -\frac{qx}{4\pi\varepsilon_0\varepsilon_1} \left(\frac{-1}{r_1^2} + \frac{\varepsilon_2 - \varepsilon_1}{\varepsilon_1 + \varepsilon_2} \frac{1}{r_2^2} \right), \qquad (12a)$$

$$E_y = -\frac{\partial}{\partial y}\varphi_1 = -\frac{qy}{4\pi\varepsilon_0\varepsilon_1}\left(\frac{-1}{r_1^2} + \frac{\varepsilon_2 - \varepsilon_1}{\varepsilon_1 + \varepsilon_2}\frac{1}{r_2^2}\right), \quad (12b)$$

$$E_z = -\frac{\partial}{\partial z}\varphi_1 = -\frac{q}{4\pi\varepsilon_0\varepsilon_1}\left(-\frac{z+a}{r_1^2} + \frac{\varepsilon_2 - \varepsilon_1}{\varepsilon_1 + \varepsilon_2}\frac{z-a}{r_2^2}\right). \tag{12c}$$

At the same time, Eq. (10) was derived for a uniform electric field, so that its further modification is required. The matter is that the non-uniformity in the Gibbs energy,

$$\frac{\delta G_m}{V_m} = \frac{(\varepsilon - 1)\varepsilon_0}{2}E^2,$$

has to be averaged over the meniscus volume, and only this averaged value should be substituted into the Gibbs thermodynamic potential (10). The expression for the averaged value of non-uniform electric field obtained from Eqs. (12) looks like

$$E^2 = E_x^2 + E_y^2 + E_z^2 = \frac{q^2}{16\pi^2\varepsilon_0^2\varepsilon_1^2} \times$$

$$\times\left[(x^2 + y^2)\left(\frac{\varepsilon_2 - \varepsilon_1}{\varepsilon_1 + \varepsilon_2}\frac{1}{r_2^2} - \frac{1}{r_1^2}\right)^2 + \right.$$

$$\left. +\left(\frac{\varepsilon_2 - \varepsilon_1}{\varepsilon_1 + \varepsilon_2}\frac{z-a}{r_2^2} - \frac{z+a}{r_1^2}\right)^2\right]. \tag{13}$$

The value of E^2 depends on the shape of the meniscus and its volume V. In turn, the latter depend on the local meniscus radii of curvature. Hence, in order to determine the local bending and the position of the meniscus, it is necessary to solve a nonlinear differential equation of the second order. The results of its numerical solution are presented in the next Section.

5. Electrocapillarity Effect on the Meniscus Shape in the AFM: Direct Variational Method

Provided that the probe tip can be approximated by a spherical surface and the specimen surface by a plane, the meniscus surface can be regarded as axially symmetric with the local radius R_m depending on the altitude coordinate z (Fig. 5). Hence, the dependence $R_m(z)$ has to be sought.

While analyzing the results obtained in the previous sections, a conclusion can be drawn that the
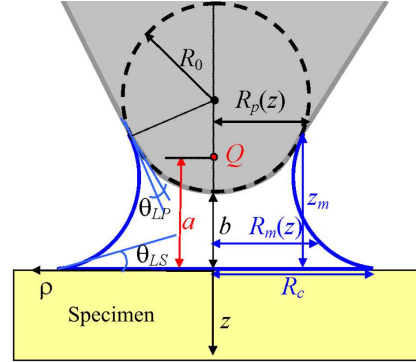

Fig. 5. Gap between the probe and the specimen after the water meniscus formation. Notations: z_m is the meniscus height, R_m is the contact radius, R_0 is the probe tip radius of curvature, b is the distance between the probe tip and the specimen surface. The electric field of the probe is simulated by the effective charge Q located at the distance a from the specimen surface

free energy of an axially symmetric meniscus with unknown shape $R_m(z)$ is a sum of several terms,

$$\Delta G[R_m(z)] = \Delta G_H + \Delta G_g + \Delta G_S + \Delta G_{\text{el}}. \tag{14}$$

The expression for the energy associated with the excess vapor pressure (humidity) looks like [6]

$$\Delta G_H = \frac{RT}{V_\mu}\ln\left(\frac{1}{H}\right)V_m \equiv$$

$$\equiv \begin{cases} \pi\dfrac{RT}{V_\mu}\ln\left(\dfrac{1}{H}\right)\displaystyle\int\limits_0^{z_m} dz R_m^2(z), & z_m < b, \\[6mm] \pi\dfrac{RT}{V_\mu}\ln\left(\dfrac{1}{H}\right)\left(\displaystyle\int\limits_0^{z_m} dz R_m^2(z) - \right. \\[4mm] \left. -\displaystyle\int\limits_b^{z_m} dz R_{tip}^2(z)\right), & z_m > b. \end{cases} \tag{15}$$

Here, $H = P/P_0$ is the relative humidity in the environment $(0 < H < 1)$. The formula for the meniscus volume V_m depends on whether the meniscus height z_m is lower or higher than the distance b between probe and the surface. In the case $z_m > b$, we have to take into account the probe volume surrounded by the meniscus, $V_p = \pi\int_b^{z_m} dz R_p^2(z)$, where the function $R_p(z)$ describes the probe shape.

The potential energy ΔG_g in the gravitation field equals

$$\Delta G_g =$$

$$= \begin{cases} \pi \rho_w g \displaystyle\int\limits_0^{z_m} R_m^2(z) z dz, & z_m < b, \\[4mm] \pi \rho_w g \left(\displaystyle\int\limits_0^{z_m} R_m^2(z) z dz - \displaystyle\int\limits_b^{z_m} R_p^2(z) z dz \right), & z_m > b, \end{cases} \quad (16)$$

where ρ_w is the water density, and $g = 9.8 \text{ m/s}^2$ is the free fall acceleration.

The surface energy ΔG_S [6] is proportional to the surface area and the surface tension coefficient. It consists of three terms,

$$\Delta G_S = \pi \gamma_{\text{LV}} S_m + \gamma_{\text{LP}} S_p + \gamma_{\text{LS}} S_c \equiv$$

$$\equiv 2\pi \gamma_{\text{LV}} \int\limits_0^{z_m} dz R_m(z) \sqrt{1 + \left(\frac{dR(z)}{dz} \right)^2} + \gamma_{\text{LP}} S_p + \gamma_{\text{LS}} S_c. \quad (17)$$

Here, γ_{LV}, γ_{LP}, and γ_{LS} are the surface tension coefficients for the liquid–vapor (LV), liquid–probe (PL), and liquid–specimen (LS) interfaces. The area of meniscus contact with the specimen equals $S_c = \pi R_c^2$. The contact area between the meniscus and the spherical probe segment is $S_p = 2\pi R_0(z_m - b)$ in the case $z_m > b$ and $S_p = 0$ in the case $z_m < b$. The areas S_c and S_p are unknown and have to be determined self-consistently. The meniscus height z_m is a single-valued function of the area S_p, the probe radius of curvature R_0, and the distance b between the probe tip and the specimen surface.

The electrostatic energy ΔG_{el} looks like

$$\Delta G_{\text{el}} =$$

$$\begin{cases} -\pi \varepsilon_0 (\varepsilon - 1) \displaystyle\int\limits_0^{z_m} dz \int\limits_0^{R_m(z)} \rho d\rho E^2(\rho, z), & z_m < b, \\[4mm] -\pi \varepsilon_0 (\varepsilon - 1) \left(\displaystyle\int\limits_0^b dz \int\limits_0^{R_m(z)} \rho d\rho E^2(\rho, z) + \right. \\[4mm] \left. + \displaystyle\int\limits_b^{z_m} dz \int\limits_{R_p(z)}^{R_m(z)} \rho d\rho E^2(\rho, z) \right), & z_m > b. \end{cases} \quad (18)$$

Here, $\varepsilon = 81$ is the relative dielectric permittivity of water, $\rho = \sqrt{x^2 + y^2}$ is the polar radius, and $E(\rho, z)$ is the probe field strength ($E^2 = E_i E_i$).

In the effective point charge models [11, 12, 14], the electric potential of the probe looks like [12]

$$\varphi = \frac{Q}{4\pi \varepsilon_0 \varepsilon} \left(\frac{\kappa - \varepsilon}{\kappa + \varepsilon} \frac{1}{r_2} - \frac{1}{r_1} \right).$$

The squared electric field strength equals

$$E^2(\rho, z) = \left(\frac{Q}{4\pi \varepsilon_0 \varepsilon} \right)^2 \left[\rho^2 \left(\frac{\kappa - \varepsilon}{\kappa + \varepsilon} \frac{1}{r_2^3} - \frac{1}{r_1^3} \right)^2 + \right.$$

$$\left. + \left(\frac{\kappa - \varepsilon}{\kappa + \varepsilon} \frac{z - a}{r_2^3} - \frac{z + a}{r_1^3} \right)^2 \right]. \quad (19)$$

Here, the effective charge Q is proportional to the voltage U applied to the probe,

$$Q(U, z_m) \approx C_t U \left[\varepsilon - (\varepsilon - 1) \exp \left(-\frac{z_m}{h_m} \right) \right],$$

C_t is the probe capacitance, and h_m the characteristic meniscus height [15]. The effective dielectric constant of the specimen that is isotropic in the transverse cross-section equals $\kappa = \sqrt{\varepsilon_{11} \varepsilon_{33}}$. The lengths of radius vectors for the real ($\mathbf{r}_1$) and image ($\mathbf{r}_2$) charges are

$$r_1 = \sqrt{\rho^2 + (z + a)^2}, \quad r_2 = \sqrt{\rho^2 + (z - a)^2}, \quad (20)$$

where a is the coordinate of the effective charge Q simulating the electric field created by the probe tip. According to the results of work [15],

$$a(z_m) = a_\infty - (a_\infty - a_0) \exp \left(-\frac{z_m}{h_m} \right),$$

where a_0 is the position of Q in the case of dry air, i.e. at $H = 0$, and a_∞ the position of Q in the case of saturated water vapor, i.e. at $H = 1$ and $z_m \to \infty$.

The Euler–Lagrange equation [16] for the unknown shape function $R_m(z)$ looks like

$$\frac{\partial g}{\partial R} - \frac{d}{dz} \frac{\partial g}{\partial (dR/dz)} = 0,$$

where g is the free energy density (see Eq. (14)). In our case, it reads

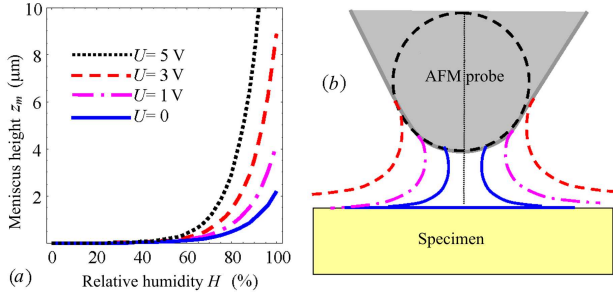$$2R_m(z) \left[\frac{RT}{V_\mu} \ln \left(\frac{1}{H} \right) + \rho_w g z \right] -$$

Fig. 6. Dependences of the meniscus height on the relative environmental humidity H for various electric voltages U applied to the AFM probe a. Meniscus shapes for various applied voltages and humidities b. Parameters used in numerical simulation calculations are quoted in Table

$$-\varepsilon_0\left(\varepsilon-1\right)R_m(z)E^2\left(R_m(z),z\right)+$$

$$+2\gamma_{\mathrm{LV}}\left[\sqrt{1+\left(\frac{dR_m}{dz}\right)^2}-\frac{d}{dz}\frac{R_m(dR_m/dz)}{\sqrt{1+(dR_m/dz)^2}}\right]=0. \tag{21}$$

Equation (21) is a nonlinear differential equation of the second order for the function $R_m(z)$. The nonlinearity is provided by the second term, which is responsible for the electrocapillarity action, and the third one describing the contribution made by the meniscus surface energy. The first term is associated with the excess vapor pressure and the gravitation force; it is linear in $R_m(z)$. Note that the contributions made by electrocapillarity and gravitation have opposite signs. Simple estimations testify that, in the overwhelming majority of cases, the contribution of the gravitation force can be neglected in comparison with the energy of excess vapor pressure, because the inequality

$$R_m(z)\frac{RT}{V_\mu}\ln\left(\frac{1}{H}\right)\gg\rho_w g z_m$$

Parameter	γ_{LV}, mN/m	ε ε	R_0, nm	b, nm	a, nm	ρ_w, kg/m^3	κ
Value *	72	81	50	10	20	10^3	$10-\infty$

* All data correspond to a room temperature of 20 °C. There is a relation $\gamma_{\mathrm{PV}}=\gamma_{\mathrm{LV}}+\gamma_{\mathrm{LP}}\cos(\theta_{\mathrm{LP}})$ between the wetting angles and then surface tension coefficients [7]. At the complete wetting, $\theta_{\mathrm{LS}}\approx\theta_{\mathrm{LP}}\approx0$.

is satisfied at $z_m<10\ \mu$m and the humidity $H<0.9$. If the electric field is applied, its energy dominates at high electric voltages. Note that, in the space regions where the derivative dR/dz can be neglected, Eq. (21) acquires a form similar to that of the modified Kelvin equation (10), namely,

$$2\rho_w\left(\frac{RT}{V_\mu}\ln\left(\frac{1}{H}\right)+gz\right)-\varepsilon_0(\varepsilon-1)E^2(R_m(z),z)=$$

$$=-\frac{2\gamma_{\mathrm{LV}}}{R_m(z)}. \tag{22}$$

In the general case, the derivative dR/dz cannot be neglected, especially near the points, where the meniscus contacts the probe and the specimen surface, so that the differential equation (21) has to be solved. Two boundary conditions should be given. They fix the wetting angles at the circular boundaries of the contact between the meniscus and the surface (θ_{LS} at $z=0$ and $\rho=R_c$), and the meniscus and the probe (θ_{LP} at $z=z_m$ and $\rho=R_p$); those angles are tabulated data [17]. Hence, the boundary conditions look like

$$\left.\frac{dR_m/dz}{\sqrt{1+(dR_m/dz)^2}}\right|_{z=0}=\cos\theta_{\mathrm{LS}},$$

$$\left.\frac{\sqrt{R_0^2-(z_m-b)^2}-(z_m-b)(dR_m/dz)}{R_0\sqrt{1+(dR_m/dz)^2}}\right|_{z=z_m}= \tag{23}$$

$$=\cos\theta_{\mathrm{LP}}.$$

As for Eq. (23), we used the geometric reasoning, according to which the vector $\mathbf{n}$ normal to the sphere has the components

$$\mathbf{n}=\frac{1}{\sqrt{1+(1-(z_m-b)/R_0)^2}}(z_m-b,R_0).$$

The solution of the boundary problem (21)–(23) depends on the meniscus height z_m. The latter can be determined afterward by minimizing functional (14), in which one must take into account that $S_p=2\pi R_0(z_m-b)$. Actually, z_m is the Lagrange multiplier.

The physical analysis of numerical solutions of the boundary problem (21)–(23) brought us to the following results. The shape of a water meniscus (at $z_m>b$) or hump (at $z_m<b$) is governed by the

air humidity H, the distance b between the probe tip and the specimen surface, the electric voltage U applied to the probe, and other geometric and material parameters, which are indicated in Table. For the hydrophilic specimen and probe surfaces, i.e. in the case $\theta_{LS} < 90°$ and $\theta_{LP} < 90°$, and for a non-zero voltage U, a small water hump always emerges on the surface at first. However, if the distance between the probe and the surface does not exceed a value of an order of 100 nm (probably, a certain critical value may exist in this case; however, almost in all experiments, this distance did not exceed tens of nanometers, so that its exact value is not essential) and the humidity exceeds a critical value, which is maximum at $U = 0$ and rapidly decreases as U grows, there emerges a water meniscus instead of a hump. The meniscus parameters do not depend on the sign of U, because the squared electric field strength enters Eq. (21). For the parameters quoted in Table, the meniscus height rapidly grows in the humidity interval $40\% < H < 70\%$ and reaches values from several hundreds of nanometers at $U = 0$ to 10 μm at $U = 5$ V (Fig. 6, *a*). The dependence of the meniscus height z_m on the humidity H is very steep (quasiexponential) at a fixed voltage U. The meniscus shape deviates more and more from the spherical one, when the applied voltage and the humidity grow, and it is the increase of the electric voltage that gives rise to the shape modification (Fig. 6, *b*).

6. Comparison with Experimental Results

The experimental dependences [3] of the meniscus height on the relative air humidity H are shown in Fig. 7, *a*. In the cited experiment, no electric voltage was applied to the probe ($U = 0$), but the air humidity and the specimen material were varied. In Fig. 7, *a*, the circles correspond to the meniscus height between a SiN probe tip and a Si specimen, and the squares to the meniscus height between a SiN probe tip and an Au specimen. The measurement error considerably grows for higher humidity values. The dotted curves were calculated theoretically from Eq. (21) for various dielectric permittivities ε of the specimen: $\varepsilon = 11.68$ for Si and $\varepsilon \to \infty$ for Au. Wetting for those substances can be regarded as almost complete. The calculated dependences qualitatively and quantitatively describe the experimental dependences of the meniscus height on the humidity obtained for both types of specimens.
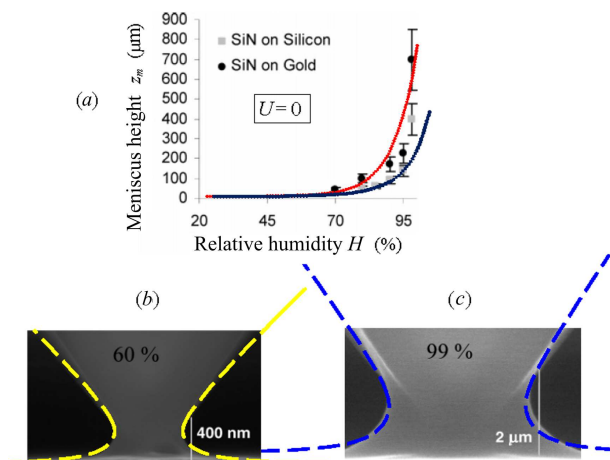

Fig. 7. Dependences of the meniscus height under the AFM probe on the relative humidity H meniscus. Symbols correspond to experimental data for the meniscus height between a SiN probe tip and a Si (circles) or Au (squares) specimen at $U = 0$ [3]. The dotted curves were calculated us theoretically from Eq. (21) for various dielectric permittivities of the specimens: $\varepsilon = 11.68$ (Si) and $\varepsilon \to \infty$ (Au). Meniscus images obtained at a humidity of 60 (*b*) and 99% (*c*). The dashed curves were calculated theoretically from Eq. (21)

The meniscus images obtained experimentally [3] at a humidity values of 60 and 99% are shown in Figs. 7, *b* and *c*, respectively. The dashed curves were calculated theoretically from Eq. (21) for Si and Au specimens. One can see that the meniscus shapes calculated theoretically agree well with the experimental ones.

7. Conclusions

To summarize, the electrocapillarity phenomena in AFM experiments, which attract attention nowadays, have been studied. In particular, the conditions required for a water meniscus to emerge in the gap between the hydrophilic surfaces of a nano-sized AFM probe tip and an examined specimen are considered. For the first time, the influence of such a specific factor as a strong non-uniformity of the electric field created by the AFM probe on the emergence conditions, the dimensions, and the shape of a water meniscus was analyzed. Moreover, for the first time, the Euler–Lagrange partial differential equation and the corresponding boundary conditions are derived, which involve the non-uniform electric field of the AFM probe, gravitation forces, the meniscus sur-

face tension, and the environmental humidity and describe the process of formation, the dimensions, and the water meniscus shape self-consistently. A direct variational method of solution of the Euler–Lagrange equation is proposed. The dependence of the local radius of the axially symmetric meniscus on its altitude coordinate is selected as the sought function. In this case, the maximum meniscus height is a variational parameter, which is determined by minimizing the energy functional of the meniscus in external fields. The obtained numerical results agree well with available experimental data.

1. S.V. Kalinin, A.N. Morozovska, Long Qing Chen, and B.J. Rodriguez, Rep. Prog. Phys. **73**, 056502 (2010).
2. A.N. Morozovska, G.S. Svechnikov, and E.A. Eliseev, *Theory of Local Polar Properties of Ferroelectrics* (Astroprint, Odessa, 2013) (in Russian).
3. B.L. Weeks, M.W. Vaughn, and J.J. DeYoreo, Langmuir **21**, 8096 (2005).
4. Th. Stifter, O. Marti, and B. Bhushan, Phys. Rev. B **62**, 13667 (2000).
5. H.-J. Butt, M.B. Untch, A. Golriz, S.A. Pihan, and R. Berger, Phys. Rev. E **83**, 061604 (2011).
6. S. Gomez-Monivas and J.J. Saenz, Phys. Rev. Lett. **91**, 056101 (2003).
7. Yu.V. Goryunov and B.D. Summ, *Wetting* (Znanie, Moscow, 1972) (in Russian); A.D. Zimon, *Fluid Adhesion and Wetting* (Khimiya, Moscow, 1974) (in Russian).
8. L.D. Landau and E.M. Lifshitz, *Statistical Physics, Part 1* (Pergamon Press, Oxford, 1980).
9. J.N. Israelachvili, *Intermolecular and Surface Science* (Academic Press, London, 1991).
10. http://en.wikipedia.org/wiki/Kelvin_equation, https://en.wikipedia.org/wiki/Young-Laplace_equation.
11. E.A. Eliseev, S.V. Kalinin, S. Jesse, S.L. Bravina, and A.N. Morozovska, J. Appl. Phys. **102**, 014109 (2007).
12. E.J. Mele, Am. J. Phys. **69**, 557 (2001).
13. V.V. Batygin and I.N. Toptygin, *Collection of Problems in Electrodynamics* (Nauka, Moscow, 1970) (in Russian).
14. A.N. Morozovska, E.A. Eliseev, and S.V. Kalinin, J. Appl. Phys. **102**, 074105 (2007).
15. A.V. Ievlev, A.N. Morozovska, V.Ya. Shur, and S.V. Kalinin, Appl. Phys. Lett. **104**, 092908 (2014).
16. L. Elsgolts, *Differential Equations and the Calculus of Variations* (Mir Publishers, Moscow, 1970).
17. P.-G. de Gennes, Usp. Fiz. Nauk **151**, 619 (1987).

Є.А. Єлісеєв

ВПЛИВ ЕЛЕКТРОКАПІЛЯРНОСТІ
НА ФОРМУ ВОДЯНОГО МЕНІСКА
В АТОМНО-СИЛОВІЙ МІКРОСКОПІЇ

Р е з ю м е

В роботі розглянуті актуальні питання аналітичної теорії явищ електрокапілярності, що виникають в АСМ-експерименті, а саме утворення водяного меніска під зондом АСМ та досліджено вплив прикладеної електричної напруги. Враховано явища електрокапілярності в неоднорідному електричному полі зонда АСМ, впливу сили тяжіння на висоту меніска та його поверхневу енергію в залежності від реальної форми, що має знаходитися самоузгодженим чином. Вперше проаналізовано вплив такого специфічного фактора, як сильна неоднорідність електричного поля зонда, на умови виникнення, розміри та форму водяного меніска. З урахуванням неоднорідного електричного поля зонда АСМ, сили тяжіння, сили поверхневого натягу меніска та вологості оточуючого середовища виведено диференційне рівняння Ейлера–Лагранжа в частинних похідних з граничними умовами, яке описує термодинаміку утворення водяного меніска самоузгодженим чином. Одержані чисельні результати описують відомі експериментальні дані.